Preprint Title Bifunctional superconducting cell as flux qubit and neuron

Authors Dmitrii S. Pashin, Pavel V. Pikunov, Marina V. Bastrakova, Andrey E. Schegolev, Nikolay V. Klenov and Igor I. Soloviev

Publication Date 01 Sep. 2023

Article Type Full Research Paper

ORCID® iDs Andrey E. Schegolev - https://orcid.org/0000-0002-5381-3297; Nikolay V. Klenov - https://orcid.org/0000-0001-6265-3670

Bifunctional superconducting cell as flux qubit and neuron

Dmitrii S. Pashin[1], Pavel V. Pikunov[1], Marina V. Bastrakova[1,2], Andrey E. Schegolev[3,4], Nikolay V. Klenov*[5,6] and Igor I. Soloviev[3,6]

Address: [1]Faculty of Physics, Lobachevsky State University of Nizhni Novgorod, 603022 Nizhny Novgorod, Russia; [2]Russian Quantum Center, 143025 Skolkovo, Moscow, Russia; [3]Skobeltsyn Institute of Nuclear Physics, Lomonosov Moscow State University, 119991 Moscow, Russia; [4]Moscow Technical University of Communication and Informatics (MTUCI), 111024 Moscow, Russia; [5]Faculty of Physics, Lomonosov Moscow State University, 119991 Moscow, Russia and [6]National University of Science and Technology MISIS, 119049 Moscow, Russia

Email: Nikolay V. Klenov - nvklenov@mail.ru

* Corresponding author

Abstract

Josephson digital or analog ancillary circuits are an essential part of a large number of modern quantum processors. The natural candidate for the basis of tuning, coupling, and neromorphic co-processing elements for processors based on flux qubits is the adiabatic (reversible) superconducting logic cell. Using the simplest implementation of such a cell as an example, we have investigated the conditions under which it can optionally operate as an auxiliary qubit while maintaining its "classical" neural functionality. The performance and temperature regime estimates obtained confirm the possibility of practical use of a single-contact inductively shunted interferometer in a quantum mode in adjustment circuits for q-processors.

Keywords

superconducting quantum computers; flux qubit; adiabatic logic cell; superconducting quantum interferometer; quantum parametron; quantum neuron; Josephson junction.

Introduction

Superconducting interferometers are widely used both as flux qubits and as a part of the peripherals in various implementations of quantum computers [1-10]. In particular, the D-Wave 2000Q quantum computer, released in 2017, operates on the principle of quantum annealing and contained a superconducting chip with 128,472 Josephson junctions, 75 percents of which were dedicated to superconducting digital electronics for controlling the processor and reading out the result, while the rest were either for qubit junctions or interconnects that allow programmable interaction between qubits. The Pegasus P16 superconducting chip of the Advantage QA system, released in 2020, contained 1,030,000 Josephson junctions, of which only 40,484 were used for interconnects and 5,640 Josephson structures were part of the qubits. In this context, designers' desire to find additional uses for multiple "auxiliary" interferometers on a chip is understandable.

The least "noisy" option for building the bulk of such quantum computing systems is based on the concepts of adiabatic superconducting logic (ASL), which can operate at millikelvin temperatures with zJ energy-efficiency [11-17]. In addition, the basic cells of adiabatic superconducting circuits can be used as a part of neuromorphic co-processors working in conjunction with quantum computing systems [18-26].

Furthermore, a natural extension of current progress would be the use of "quantum" degrees of freedom for adiabatic superconducting circuits, which share many similarities with qubits in terms of their representation of information via magnetic flux. From a formal point of view, the system under consideration is a superconducting circuit in a quantum state, transforming the input magnetic flux Φ_{in} into an output magnetic flux Φ_{out} according to a specific (e.g. sigmoidal) function $\Phi_{out}=f(\Phi_{in})$ [27,28]. If we only want to use the circuit in the "classical" neuromorphic mode the transfer characteristic should be such that small fluctuations at the input do not produce a noticeable response, but above a certain threshold, any signal at the input produces a fixed magnetic flux at the output. And if it were possible to adapt the ASL cell in a perceptron to process the signal from a qubit representing its quantum state restructuring the one's spectrum in a certain way, we would have an auxiliary qubit that neither requires a highly stable reference oscillator nor a mixer to drive it. Of course, such a bifunctional cell as a qubit is not ideal, however in some situations the gain in the "payload" on the chip may be more important.

Apparently, the simplest superconducting circuit with a nonlinear flux-to-flux transformation in the classical regime is a single-contact interferometer, as depicted in the left part of figure 1. However, the typical form of the function f for such an element does not meet the aforementioned requirements. In the classical mode, it can be demonstrated [22] that the desired form of $f(\Phi_{in})$ can be achieved by adding an inductance with a specially chosen linear flux-to-flux transformation to the interferometer, as illustrated in the right part of 1. At zero temperature and under quasi-adiabatic changes in the circuit's inputs, the desired transformation (now for average values) will occur even in the quantum regime, when the spectrum of eigenvalues of the system's Hamiltonian operator is discrete. Nevertheless, it raises the question of how will the proposed adjustment circuit operate at finite (millikelvin) temperatures in the quantum regime and under the influence of relatively fast magnetic field control pulses? Won't the tuning, coupling, and neromorphic co-processing circuits acquire new useful properties in the quantum regime?

This article is devoted to the search for answers to these questions. Hence, below we explore the quantum dynamics of observables in superconducting interferometers, discuss the implications for quantum computing, and the challenges that remain to be addressed. In addition, we note the potential for utilizing the findings to develop components of neuromorphic co-processors that collaborate with quantum computing systems. Also the corresponding cell (a single-contact interferometer shunted by inductance as depicted in figure 1) further in the text we will refer to as the *parametron*.

The model of the proposed bifunctional cell

In this and subsequent sections, we consider a parametric quantron (parametron) under the influence of unipolar pulses of external magnetic flux. It should be noted that this system has proven to be a basic element of neural networks such as the perceptron with a sigmoidal input-to-output transformation function (sigma-neuron). Preliminary calculations have shown that, under cer-

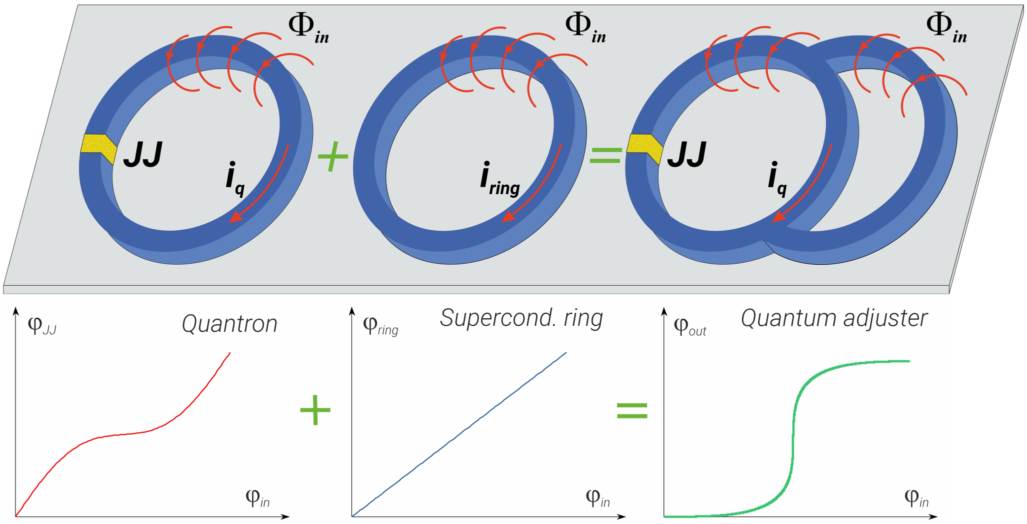

Figure 1: The idea behind the creation of the *bifunctional cell*: the combination of a quantum interferometer (quantron) and a simple superconducting ring leads to the emergence of a parametron with a sigma-like transfer function. $\varphi_{in}(t)$ and $\varphi_{out}(t)$ are the normalised fluxes at the input and output of the circuit ($\varphi_{out}(t)$ corresponds to the current i_q). Nota Bene: such a transfer characteristic is a good activation function for a neuron in a perceptron-type network, suitable for primary signal processing for quantum computing systems.

tain conditions, such a neuron can operate successfully in both classical and quantum modes [18,20,22,23,25]. The energy of the system in the Hamiltonian formalism can be expressed as follows:

$$H_{sys}(t) = \frac{E_c p^2}{\hbar^2} + E_J \left\{ \frac{(b\varphi_{in}(t) - a\varphi)^2}{2a} + (1 - \cos\varphi) \right\}, \tag{1}$$

where coefficients a and b are defined by the following expressions [22,25]:

$$a = \frac{l_a + l_{out}}{l l_{out} + l_{out}(l + l_a)}, \quad b = \frac{l_a + 2l_{out}}{2\left[l l_a + l_{out}(l + l_a)\right]}, \quad l_a = 1 + l. \tag{2}$$

Here l is the normalised inductance of the quantron part of sigma-interferometer ($l = 2\pi L I_C/\Phi_0$), l_a is the additional linear inductance, and l_{out} is the output inductance (l_a and l_{out} are normalised in the same manner as l).

To investigate the flux-to-flux transfer characteristics of such a system, it is convenient to interpret its evolution as the movement of a particle with mass $M = \frac{\hbar^2}{2E_c}$ and momentum $p = -i\hbar\frac{\partial}{\partial\varphi}$ in the potential profile defined by the second term in (1). Wherein the effective coordinate is a phase of the Josephson junction, φ. Quantities $E_C = \frac{(2e)^2}{2C}$ and $E_J = \frac{I_C \Phi_0}{2\pi}$ are capacitive and Josephson energies respectively, determined by the Josephson junction's critical current I_C and capacity C. A typical example of "flux-based" system state management is provided by the dynamically varying input magnetic flux:

$$\varphi_{in}(t) = A\left[\left(1 + e^{-2D_R(t-t_1)}\right)^{-1} + \left(1 + e^{2D_F(t-t_2)}\right)^{-1}\right] - A. \tag{3}$$

This flux pulse is characterised by the level A, rise/fall rate of the signal $D_{R/F}$ and characteristic times t_1 and $t_2 = 3t_1$, responsible for the rise and fall periods of input magnetic flux. It is assumed that the time is given in units of ω_p^{-1}, where $\hbar\omega_p \equiv \sqrt{2E_J E_C}$.

In the framework of the adiabatic approach one can numerically find "instantaneous" energy levels $E_n(t)$ and "instantaneous" eigenwave functions $|\psi_n(t)\rangle$ of the system solving the stationary Schrödinger equation:

$$H_{sys}(t)|\psi_n(t)\rangle = E_n(t)|\psi_n(t)\rangle. \tag{4}$$

If at each moment of time the state energy $E_n(t)$ is much smaller than the distance between energy levels in the system, then the adiabatic approximation is valid and, therefore, transitions between instantaneous eigenstates can be neglected. Mathematically this condition can be expressed as:

$$\left|\langle E_n(t)\left|\frac{d}{dt}\right|E_m(t)\rangle\right| \ll \left|\frac{E_m(t) - E_n(t)}{\hbar}\right|, \tag{5}$$

which just defines the standard Landau-Zener problem [29-31]. If the adiabatic approximation is violated, e.g. for the moments when the energy levels $E_n(t)$ and $E_m(t)$ converge (anticrossing), the Landau-Zener transitions occur. The rate of these transitions is controlled by the form of the external influence. At moments of level convergence for short periods τ_{LZ} the phases of the wave functions change significantly, leading to strong fluctuations of the level populations in the system and can lead to quasi-random dynamics in the parametron. In addition, Landau-Zener interference has become a tool to access the multilevel structure of these artificial atoms [32-35], and also is used to obtain information about the connection of the qubits with a noisy environment and to form dissipative stable entanglement in quantum tomography protocols [36-38]. Let's further consider the limitations that such non-adiabatic effects impose on the potential use of the proposed cell as a neuromorphic, coupling, and tuning element in quantum computing systems. At the same time, we will also gain an understanding of the possibilities for controlling the population of levels in the simplest implementation of an adiabatic superconducting logic cell when used as an auxiliary qubit.

The performance limitations due to Landau-Zener transitions

The states dynamic of the considered system (eq. 1) is primarily defined by features of the controlling field (eq. 3), as well as by values of inductances. We have carried out two cases of external field influence to the system: when the controlling field has symmetrical rise/fall fronts, $D_R = D_F = D$, and when it hasn't, $D_R \neq D_F$. It is assumed that at the initial time the system is initialised to the ground state, i.e. localised at the level with energy E_0. An evolution of energy levels population and instantaneous energy levels were numerically calculated for the $N = 10$ lowest energy levels of the quantum interferometer. As shown in figure 2(a,b), during the rise and fall of the field, the instantaneous energy levels are getting closer and the anti-crossing effect is observed. For the ground and first-excited states characteristic times of anti-crossing corresponding to the τ_{LZ}, when the adiabatic condition (5) is violated and a non-zero probability of Landau-Zener tunneling between these energy levels is emerged. So far as the leakage to upper states (for $N > 2$) during such transitions is less than $|P_1 - P_0| \gg P_{N \geq 2}$, the two-levels approximation ($N = 2$) could be applied for analytical estimations of Landau-Zener transitions probabilities [32,35]. Within this approximation, the system can be approximated by the following Hamiltonian:

$$\bar{H}_{sys}(\tau_{LZ}) = \frac{1}{2}\begin{pmatrix} \epsilon(\tau_{LZ}) & \Delta \\ \Delta & -\epsilon(\tau_{LZ}) \end{pmatrix} \tag{6}$$

where $\Delta = E_1(t_{LZ}) - E_0(t_{LZ})$ determined the distance between energy levels at the moment of their closest convergence, and $\epsilon(\tau_{LZ})$ determined the type of levels anti-crossing. The instantaneous energy levels of the ground and excited states can then be written as $E_{0,1}(\tau_{LZ}) = \pm\frac{1}{2}\sqrt{\Delta^2 + \epsilon^2(\tau_{LZ})}$. Let us estimate the Landau-Zener transition probability at the moment of the first levels convergence, which corresponding to the time t_{LZ} for diabatic dynamic (when $\Delta \to 0$) of levels crossing (dashed lines in inserts in figure 2 (a,b)). As clearly seen from the simulation, anti-crossing effect occurs on small time scales near the moment of convergence t_{LZ}. This allows us to use linear approximation on time $\epsilon(t_{LZ} + \tau_{LZ}) \approx \epsilon'(t_{LZ}) \cdot \tau_{LZ}$ and write the Hamiltonian of the system as:

$$\bar{H}_{sys}(t_{LZ} + \tau_{LZ}) \approx \bar{H}_{sys}(t_{LZ}) + V(\tau_{LZ}), \tag{7}$$

meanwhile, we believe that $V(\tau_{LZ}) = -\frac{1}{2}A \cdot D \cdot b\varphi\tau_{LZ}$ is small on the scale of the Landau-Zener transition time, and this allows us to use the perturbation theory to estimate the value of $\epsilon'(t_{LZ})$. In the moment of anti-crossing instantaneous energy levels E_0 and E_1 are reaching their extremum, therefore it is necessary to take into consideration the second order of perturbation theory for analytical estimation of convergence value:

$$E_{1,0}(t_{LZ} + \tau_{LZ}) \approx \pm\frac{\Delta}{2} \pm \frac{|V_{01}(\tau_{LZ})|^2}{\Delta}, \tag{8}$$

where $V_{01}(\tau_{LZ}) \equiv \langle\psi_0(t_{LZ})|V(\tau_{LZ})|\psi_1(t_{LZ})\rangle$. Finally from (eq. 8) the difference between energy levels is

$$E_1(t_{LZ} + \tau_{LZ}) - E_0(t_{LZ} + \tau_{LZ}) \approx \Delta + \frac{2|V_{01}(\tau_{LZ})|^2}{\Delta}. \tag{9}$$

On the other side, expanding in the row up to the second order, we can get the difference between the levels:

$$E_1(t_{LZ}+\tau_{LZ}) - E_0(t_{LZ}+\tau_{LZ}) \approx \Delta + \frac{\epsilon'^2(t_{LZ})}{2\Delta}\tau_{LZ}^2. \tag{10}$$

Then from Eqs. (9) and (10) obtain:

$$\epsilon'(t_{LZ}) = AD \cdot b|\langle\psi_0(t_{LZ})|\varphi|\psi_1(t_{LZ})\rangle|. \tag{11}$$

The dots in the insets to fig. 2(a,b) show the behavior of the adiabatic energy levels at the anti-crossing τ_{LZ}. The estimates calculated in the framework of the two-level model are in good agreement with the numerical calculations (whole lines in figure 2(a,b)). This agreement indicates the correctness of the approximations used for the estimation. Based on the resulting expression for the linear coefficient expression (11) for $\epsilon(t_{LZ}+\tau_{LZ})$, we use the well-known formula for calculating the probability of Landau-Zener transitions [32,35] with a single convergence of the levels:

$$P_{LZ} = e^{-2\pi\Gamma}, \quad \Gamma \equiv -\frac{\pi\Delta^2}{2\hbar AD \cdot b|\langle\psi_0(t_{LZ})|\varphi|\psi_1(t_{LZ})\rangle|}. \tag{12}$$

Using the obtained formula (12), we estimate the limit of occurrence of Landau-Zener transitions for different parameters of the control field and inductances in the circuit. To do this, we have calculated the interference probability maps of the populations of the first excited level for typical quantum well inductances l and different parameters $D_{R,F}$ for symmetric (fig. 2(c)) and asymmetric (fig. 2(d)) external control fields at the time corresponding to the end of the external influence. Bright areas in figure 2(c,d) correspond to regions where there is a non-zero probability of quantum-coherent Landau-Zener tunneling, and black areas correspond to the adiabatic control of the system. According to the expressions (12), the white dashed line in figure 2(c) denotes the limit of the transition probability from the ground to the excited state $P_{LZ} < 0.01$. This estimate is important for evaluating the functioning of this circuit in adiabatic quantum neural networks, where there are strict requirements for the absence of excitation from the initial state for the implementation of sigmoidal activation functions [25].

We can see from fig. 2(e) that for the symmetric control field for given $D_{R,F}$ there are ranges of inductance values l where we can control the populations of levels by external influence using the Landau-Zener tunneling effect. In other words, in this parameter range we can, if necessary, control the state of the simplest adiabatic cell used as an auxiliary qubit. This parameter range is also important for the observation of quantum non-perturbative effects for the parametron acting as a nonlinear adjuster implementing the interaction between fluxonium type qubits [39,40]. In the case of an asymmetric control field, see fig. 2(f), there is no complete transition between the E_0 and E_1 states in the system for a wide range of inductances, indicating the practical expediency of using a symmetric control influence. Another way of controlling the change in the level populations in the system is to control the phase difference between a pair of converging levels in the regions of increase (or decrease) in the external field, which of course depends on $\Delta t = t_2 - t_1$. These dependencies are naturally periodic, as shown in fig. 2(g,h), for two cases of application of an external field.

The action time of the symmetric input flux to avoid Landau-Zener transitions is $\sim$ 100 ns for $l = 2$. An estimate was made with the characteristic parameters of the Josephson junction: $I_C = 50$ nA and $C = 6$ fF. On the other hand it takes $\sim$ 30 ns for transition from the ground state to the first excited state, as shown in fig. 2(a). It can be assumed that the characteristic duration of the "NOT" operation will be of the same order of magnitude for the "flux control" of the tuning circuit cell used as an auxiliary qubit. We have evaluated the reliability of such an operation based on the calculation of fidelity. We evaluate the fidelity of the gate U_g (for fig. 2(a)) as in [41]:

$$F = \frac{1}{6} \sum_{|\alpha\rangle \in \nu} \left| \langle \alpha | U_g^{\dagger} U_{id} | \alpha \rangle \right|^2, \tag{13}$$

where the summation runs over the six states ν aligned along the cardinal directions of the Bloch sphere $|x_{\pm}\rangle = \dfrac{|0\rangle \pm |1\rangle}{\sqrt{2}}$, $|y_{\pm}\rangle = \dfrac{|0\rangle \pm i|1\rangle}{\sqrt{2}}$, $|z_{+}\rangle = |0\rangle$, $|z_{-}\rangle = |1\rangle$. Here $|0\rangle$ and $|1\rangle$ are the ground and first excited state of the system, U_{id} is the matrix of an ideal qubit gate. For the "NOT" operation, for example, shown in fig. 2(a) for $l = 2.63$ and $D = 0.0044$, taking into account the optimization of the pulse parameters Δt, according to fig. 2(g), we can get the fidelity of the operation $F = 99.99\%$.

A model for dissipative effects in the bifunctional cell

Another important aspect to consider is the investigation of the impact of dissipative and temperature effects on the nonlinear dynamics of quantum interferometers. Quantum noise can result in the breakdown of coherence in the system and affect the operation of parametron within coupling circuits and tuning schemes. In order to accurately describe these processes, we present the complete Hamiltonian of the system as:

$$H = H_{sys}(t) + H_R + H_{int}, \tag{14}$$

where $H_{sys}(t)$ is defined by the expression (1), H_R is the energy of the thermal bosonic reservoir of the form:

$$H_R = \sum_i \hbar\Omega_i b_i^\dagger b_i, \tag{15}$$

where Ω_i is a frequency of the i^{th} bosonic mode, $b_i^\dagger$ and b_i are creation and annihilation operators for the i^{th} bosonic mode. H_{int} is responsible for the interaction between the thermostat and superconducting parametron. So for the case of ohmic dissipation this relationship is linear and can be written as:

$$H_{int} = k\varphi \sum_i \left(b_i^\dagger + b_i\right), \tag{16}$$

where k is a coupling constant.

Within the framework of the adiabatic approximation we can form the density matrix of the system in the instantaneous basis $|\psi_n(t)\rangle$ as

$$\rho(t) = \sum_{m,n} \rho_{mn}(t)\, |\psi_m(t)\,\rangle\langle\,\psi_n(t)| \,. \tag{17}$$

In the Born-Markov approximation the dissipative dynamic of a quantum system is described by an adiabatic generalised equation for the density matrix [42]. In terms of the instantaneous basis in Schrödinger representation parametron's dynamics obeys the Redfield equation:

$$\dot{\rho}(t) = -i[H(t), \rho(t)] + k^2 \sum_{n,m} G(\omega_{mn})[[L_{nm}, \rho(t)], \varphi], \tag{18}$$

$$\text{with} \quad G(\omega_{mn}) = \pi g\big(\theta(\omega_{mn})(\bar{n}(\omega_{mn}) + 1) + \theta(\omega_{nm})\bar{n}(\omega_{nm})\big)$$

$$\text{and} \quad L_{nm} = |\psi_n(t)\,\rangle\langle\,\psi_m(t)|\,\langle\psi_n(t)\,|\varphi|\,\psi_m(t)\rangle \,.$$

Here, we are not taking into account Lamb shifts; g is the density of bosonic modes, θ is the Heaviside function, and $\bar{n}(\omega) = \frac{1}{e^{\hbar\omega/k_B T}-1}$ is the Planck distribution (k_B is the Boltzmann constant).

It should be noted that equation (18) is valid under the standard adiabatic condition: $h/\delta^2 \ll 1$,

$$\text{where} \quad \delta = \min_t(E_1(t) - E_0(t)) \quad \text{and} \quad h = \max_{t,n,m} \left|\left\langle\psi_n(t)\left|\partial_t H_{sys}(t)\right|\psi_m(t)\right\rangle\right| .$$

The ratio $h/\delta^2 \approx 0.08$ for characteristic parameters $l = 2$, $D = 0.001$.

We will apply the described model to analyze the limitations on the operating temperature range when using the proposed parametron in coupling circuits and tuning schemes in quantum computing systems.

Restrictions on operating temperature ranges for the bifunctional cell

The analysis conducted in Section 3 showed that Landau-Zener transitions significantly affect the dynamics of the system. Even in the case of adiabatic control, relaxation and thermal excitation processes can introduce additional difficulties that need to be considered when designing quantum interferometers and tuning circuits, adjusters, neurons based on them. In particular, dissipative processes significantly affect the flux-to-flux transfer characteristics of such systems. In the work [25], we demonstrated that increasing the coupling coefficient of the interferometer with the reservoir suppresses oscillations of the mean flux value (generalised coordinate) caused by interference nonadiabatic effects. However, another important factor (in addition to relaxation) that influences the evolution of observable quantities for an interferometer is thermal fluctuations. It is known that the operating temperature, T, of quantum circuits with Josephson junctions is chosen much smaller than the characteristic temperature scale given by the distance between their ground and first excited energy levels:

$$T \ll \frac{E_1(t) - E_0(t)}{k_B}. \tag{19}$$

At the same time, the probability of reaching higher energy levels is proportional to $e^{-\frac{E_1(t)-E_0(t)}{k_B T}}$, and the distance between the instantaneous energy levels depends on the applied external control field $\varphi_{in}(t)$, see 3(a). For example, for parameters $l = 2$, $D = 0.001$, corresponding to the adiabatic control region with symmetric magnetic flux (see fig. 2(c)), the energy gap between states $\min_t(E_1(t) - E_0(t))/k_B \sim 0.15\ K$ during the increasing and decreasing of the external flux is shown in fig. 3(b). During these time intervals, the condition (19) may be violated, leading to transitions to higher energy levels. Therefore, an analysis of the parameter behavior as a function of working temperature is required to find operating modes where the probability of such thermal transitions is minimised.

We focused our attention on macroscopic observables in the parametron in quantum regime, such as the transfer characteristic $i_{out} = f(\varphi_{in})$. For the considered scheme shown in fig. 1, this dependence can be expressed through the following relation:

$$i_{out} = \frac{\varphi_{in} - 2l_a\langle i\rangle}{2(l_a + l_{out})}. \tag{20}$$

Here, $\langle i\rangle = b\varphi_{in}(t) - a\langle\varphi\rangle$ is the mean value of the current operator on the Josephson junction when the external flux changes relative to the mean phase of the contact $\langle\varphi\rangle = \langle\psi(t)|\varphi|\psi(t)\rangle$. As shown in fig. 4(a), the transfer characteristic of the parametron has a sigmoidal dependence. It is worth noting that this feature allows for the use of the proposed scheme in superconducting neural networks, such as perceptrons, integrated into hybrid quantum-neuromorphic computers. Moreover, temperature affects the steepness of the sigmoid function and even the manifestation of hysteresis in flux-to-flux transformations (when $i_{out}(\varphi_{in})$ during the increase of the external signal $\varphi_{in} = 0 \Rightarrow \varphi_{in} = A$, solid lines in fig. 4(a), does not coincide with the behavior of the mean values during the decrease of the magnetic signal $\varphi_{in} = A \Rightarrow \varphi_{in} = 0$, dashed lines in fig. 4(a)). We also emphasise that the sigmoidal transfer characteristic obtained is very useful for using the adiabatic cell in question as an auxiliary qubit. This feature of the system's behaviour, together with the possibility of tuning the energy spectrum, makes it possible to minimise its parasitic "magnetic" influence on the environment.

Figure 4(b) presents the temperature map showing the maximum temperature at which the transfer characteristic of the parametron is sufficiently close to a sigmoid. To construct this map, we considered curves for which the standard deviation, SD, from the mathematical sigmoid did not exceed 10^{-4}. The ordinate and abscissa axes correspond to the rise/fall rates of the applied flux and normalised inductance of the cell, respectively. The calculations show that as the inductance of the parametron l and the performance of one increases, the requirements for system temperature control also increase, necessitating increasingly lower operating temperatures. For example, the dark blue region in fig. 4(b) is only suitable for $T \sim 0.1K$. Note that for the parameters used and the Josephson junction quality factor $Q \sim 10^5$, the relaxation time is $t_r \sim 1\ \mu s$. From this rough estimate, it can be seen that in the future adiabatic cells of tuning circuits can also be used as auxiliary qubits for a more efficient use of structures on a "quantum" chip.

Conclusions

In conclusion, the simplest cell of adiabatic superconducting logic can function even in quantum mode as an element of tuning circuits if the control signals change quasi-adiabatically with time (rise/fall times for control fields are more than a 100 ns). At sufficiently low temperatures and relatively small normalised inductances, such a shunted single-contact interferometer can also be used as part of a perceptron-type neural network to process signals received from qubits. Such a cell can be used in quantum mode also as an auxiliary qubit with relatively fast “flux” control. Future research will address the problem of using more advanced adiabatic superconducting logic cells for such purposes. In addition, bifunctional cells, which can act as adiabatic neurons or flux qubits depending on the operating conditions, have the potential to be used to simulate the operations in a non-classical brain [43].

Funding

The development of the method of analysing the evolution of observables for the adiabatic logic cells in quantum mode was carried out with the support of the Grant of the Russian Science Foundation No. 22-72-10075. The development of the main concept was carried out with the financial support of the Strategic Academic Leadership Programme “Priority-2030” (grant from NITU “MISIS” No. K2-2022-029). A.S. is grateful to the the Foundation for the Advancement of Theoretical Physics and Mathematics "BASIS" (grant 22-1-3-16-1).

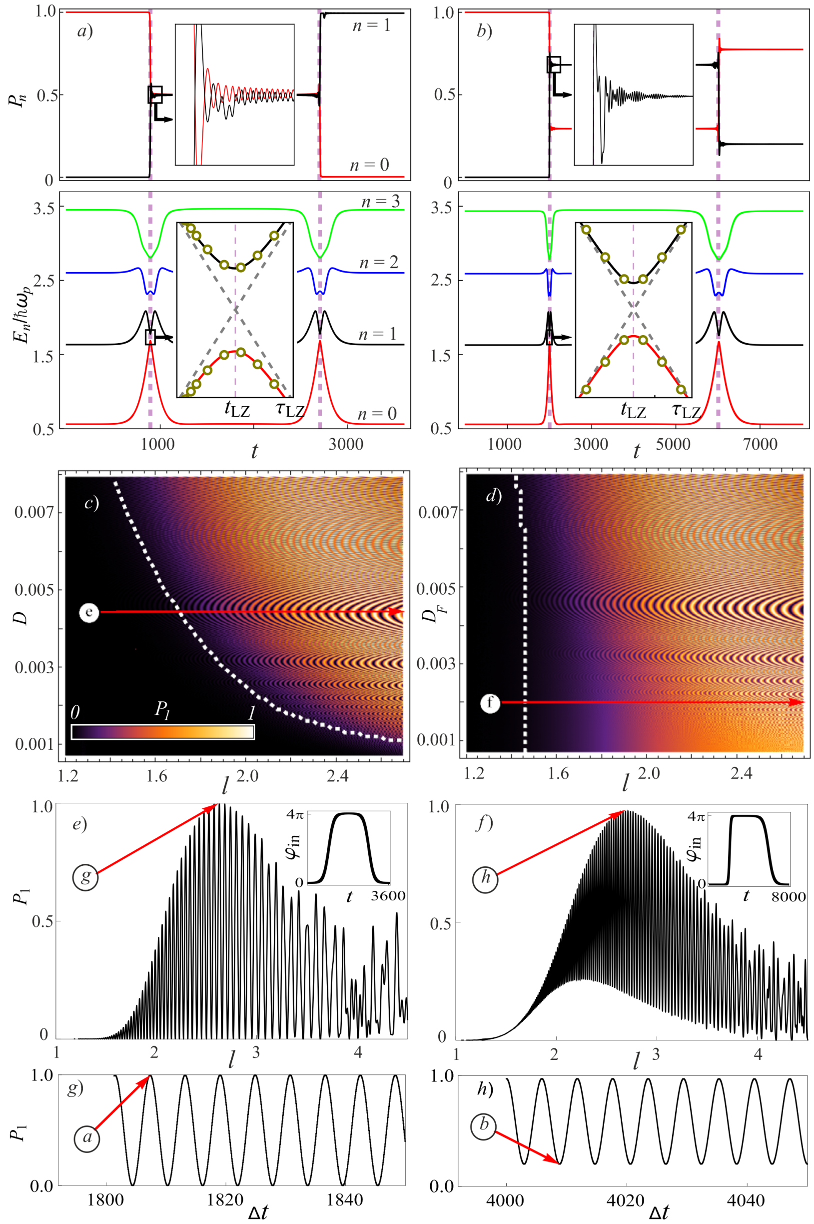

Figure 2: (a, b) The time dependence of population of the ground state, $P_0(t)$, (black curve) and first excited state, $P_1(t)$, (red curve). Additionally four lowest states $E_i(t)$ of quantum interferometer are also demonstrated for a) $l = 2.63$, b) $l = 2.69$. Diabatic levels for $E_{0,1}$ demonstrated in insert by dashed line, and analytical estimations in two-level approximation (due to the formula (10)) – by dots. (c,d) Interference population map for the first excited state for various values of the inductance l and rates of change of the control field fronts $D_{R/F}$. White dashed line denotes the violation boundary of the adiabatic approximation according to the formula (12) with accuracy equal to $P_{LZ} > 1\%$. For $D = 0.0044$ (e) and $D_R = 0.008$, $D_F = 0.002$ in (f) cross sections of probabilities $P_1(l)$ are demonstrated, which are marked with red arrows in (c,d). (g,h) Population of the excited state as a function of $\Delta t = t_2 - t_1$ with fixed a) $l = 2.69$, b) $l = 2.63$ at the end of external influence. Plots (a,c,e,g) were calculated for the symmetrical $\varphi_{in}(t)$, meanwhile (b,d,f,h) – for asymmetrical input flux. Parameters of the system were: $l_a = 1 + l$, $l_{out} = 0.1$, $E_J = 2E_c$, $t_1 = 3t_2$.

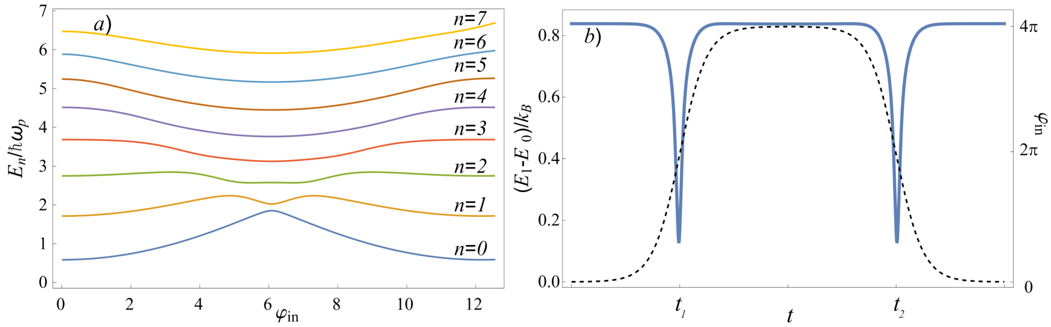

Figure 3: a) The spectrum of the Hamiltonian (1) versus the external flux $\varphi_{in}(t)$. b) (Blue solid color) The temporal dependence of the distance between the ground state, $E_0(t)$, and the first excited state, $E_1(t)$, in the instantaneous basis of the parametron in quantum regime. (Black dashed color) The dependence of the input magnetic flux φ_{in} on time. The parameters of the circuit are: $l = 2$, $D = 0.001$, $A = 4\pi$, $l_a = 1 + l$, $l_{out} = 0.1$, $E_J = 2E_c$, $t_1 = 4000$, $t_1 = 3t_2$.

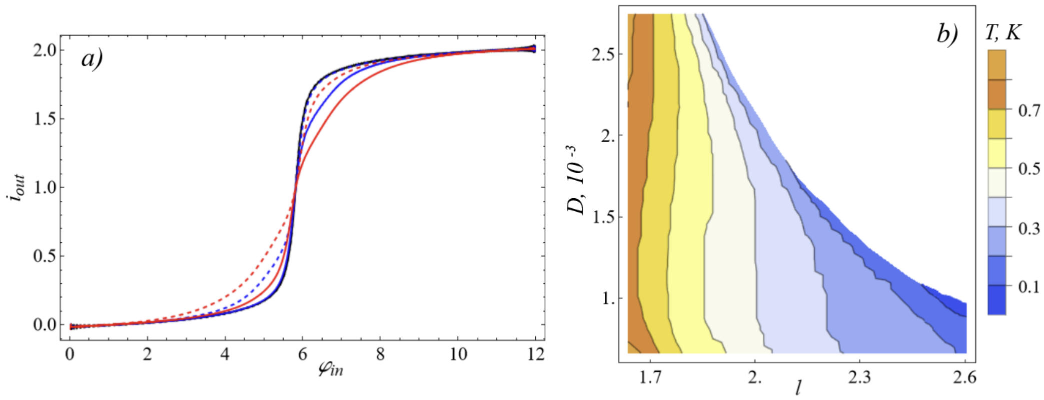

Figure 4: a) The influence of temperature on the transfer characteristic of the parametron in quantum regime : the solid lines represent the "forward" evolution of the system ($\varphi_{in} = 0 \Rightarrow \varphi_{in} = A$) and the dashed lines represent the "reverse" evolution ($\varphi_{in} = A \Rightarrow \varphi_{in} = 0$). The black curve corresponds to zero temperature, while the blue and red curves correspond to temperatures of 0.5 K and 1 K, respectively. b) The region of parameters where the transfer characteristic is close to a sigmoidal shape with a standard deviation of $SD < 10^{-4}$. In the white area even at zero temperature the standard deviation is larger then $SD = 10^{-4}$. The system parameters used in the simulation were: $A = 4\pi$, a coupling coefficient with the thermostat determined by condition $2\pi g k^2/\omega_p = 0.0025$, $l_a = 1 + l$, $l_{out} = 0.1$, $E_J = 2E_c$, and $t_1 = 3t_2$.

References

1. Dattani, N.; Szalay, S.; Chancellor, N. *arXiv preprint arXiv:1901.07636* **2019**.

2. Vyskocil, T.; Djidjev, H. *Algorithms* **2019**, *12* (4), 77.

3. Boothby, K.; Bunyk, P.; Raymond, J.; Roy, A. *arXiv preprint arXiv:2003.00133* **2020**.

4. Boothby, K.; King, A. D.; Raymond, J. *D-Wave Technical Report Series* **2021**.

5. Manucharyan, V. E.; Koch, J.; Glazman, L. I.; Devoret, M. H. *Science* **2009**, *326* (5949), 113–116.

6. Nguyen, L. B.; Lin, Y.-H.; Somoroff, A.; Mencia, R.; Grabon, N.; Manucharyan, V. E. *Physical Review X* **2019**, *9* (4), 041041.

7. Grover, J. A.; Basham, J. I.; Marakov, A.; Disseler, S. M.; Hinkey, R. T.; Khalil, M.; Stegen, Z. A.; Chamberlin, T.; DeGottardi, W.; Clarke, D. J. et al. *PRX Quantum* **2020**, *1* (2), 020314.

8. Zhang, H.; Chakram, S.; Roy, T.; Earnest, N.; Lu, Y.; Huang, Z.; Weiss, D.; Koch, J.; Schuster, D. I. *Physical Review X* **2021**, *11* (1), 011010.

9. Gyenis, A.; Mundada, P. S.; Di Paolo, A.; Hazard, T. M.; You, X.; Schuster, D. I.; Koch, J.; Blais, A.; Houck, A. A. *PRX Quantum* **2021**, *2* (1), 010339.

10. Somoroff, A.; Ficheux, Q.; Mencia, R. A.; Xiong, H.; Kuzmin, R.; Manucharyan, V. E. *Physical Review Letters* **2023**, *130* (26), 267001.

11. Takeuchi, N.; Ozawa, D.; Yamanashi, Y.; Yoshikawa, N. *Superconductor Science and Technology* **2013**, *26* (3), 035010.

12. Takeuchi, N.; Yamanashi, Y.; Yoshikawa, N. *Applied Physics Letters* **2013**, *102* (5), 052602.

13. Takeuchi, N.; Yamanashi, Y.; Yoshikawa, N. *Applied Physics Letters* **2013**, *103* (6), 062602.

14. Takeuchi, N.; Yamanashi, Y.; Yoshikawa, N. *Scientific reports* **2014**, *4* (1), 1–4.

15. He, Y.; Takeuchi, N.; Yoshikawa, N. *Applied Physics Letters* **2020**, *116* (18), 182602.

16. Ayala, C. L.; Tanaka, T.; Saito, R.; Nozoe, M.; Takeuchi, N.; Yoshikawa, N. *IEEE Journal of Solid-State Circuits* **2020**, *56* (4), 1152–1165.

17. Takeuchi, N.; Yamae, T.; Ayala, C. L.; Suzuki, H.; Yoshikawa, N. *IEICE Transactions on Electronics* **2022**, *105* (6), 251–263.

18. Schegolev, A. E.; Klenov, N. V.; Soloviev, I. I.; Tereshonok, M. V. *Beilstein Journal of Nanotechnology* **2016**, *7* (1), 1397–1403.

19. Soloviev, I. I.; Schegolev, A. E.; Klenov, N. V.; Bakurskiy, S. V.; Kupriyanov, M. Y.; Tereshonok, M. V.; Shadrin, A. V.; Stolyarov, V. S.; Golubov, A. A. *Journal of Applied Physics* **2018**, *124* (15), 152113.

20. Schegolev, A.; Klenov, N.; Soloviev, I.; Tereshonok, M. *Superconductor Science and Technology* **2021**, *34* (1), 015006.

21. Bakurskiy, S.; Kupriyanov, M.; Klenov, N. V.; Soloviev, I.; Schegolev, A.; Morari, R.; Khaydukov, Y.; Sidorenko, A. S. *Beilstein journal of nanotechnology* **2020**, *11* (1), 1336–1345.

22. Bastrakova, M.; Gorchavkina, A.; Schegolev, A.; Klenov, N.; Soloviev, I.; Satanin, A.; Tereshonok, M. *Symmetry* **2021**, *13* (9), 1735.

23. Gorchavkina, A.; Bastrakova, M.; Klenov, N.; Satanin, A. Monte Carlo simulations of the switching processes in the superconducting quantron-based neuron. In *Journal of Physics: Conference Series*; 2021; p 012063.

24. Schegolev, A. E.; Klenov, N. V.; Bakurskiy, S. V.; Soloviev, I. I.; Kupriyanov, M. Y.; Tereshonok, M. V.; Sidorenko, A. S. *Beilstein Journal of Nanotechnology* **2022**, *13* (1), 444–454.

25. Bastrakova, M. V.; Pashin, D. S.; Rybin, D. A.; Schegolev, A. E.; Klenov, N. V.; Soloviev, I. I.; Gorchavkina, A. A.; Satanin, A. M. *Beilstein Journal of Nanotechnology* **2022**, *13* (1), 653–665.

26. Islam, M. M.; Alam, S.; Hossain, M. S.; Roy, K.; Aziz, A. *Journal of Applied Physics* **2023**, *133* (7), 070701.

27. Liu, Y.-x.; Wei, L.; Tsai, J.; Nori, F. *Physical review letters* **2006**, *96* (6), 067003.

28. Van der Ploeg, S.; Izmalkov, A.; van den Brink, A. M.; Hübner, U.; Grajcar, M.; Il'Ichev, E.; Meyer, H.-G.; Zagoskin, A. *Physical review letters* **2007**, *98* (5), 057004.

29. Landau, L. D. *Phys. Z. Sowjetunion* **1932**, *2*, 46.

30. Zener, C. *Proc. R. Soc. A* **1932**, *137*, 696–702.

31. Stückelberg, E. C. G. *Helv. Phys. Acta* **1932**, *5*, 369–423.

32. Shevchenko, S. N.; Ashhab, S.; Nori, F. *Physics Reports* **2010**, *492* (1), 1–30.

33. Mi, X.; Kohler, S.; Petta, J. R. *Phys. Rev. B* **2018**, *98* (16), 161404(R).

34. Denisenko, M. V.; Satanin, A. M.; Ashhab, S.; Nori, F. *Phys. Rev. B* **2012**, *85* (18), 184524.

35. Ivakhnenko, O. V.; Shevchenko, S. N.; Nori, F. *Physics Reports* **2023**, *995*, 1–89. doi:10.1016/j.physrep.2022.10.002.

36. Gramajo, A. L.; Domínguez, D.; Sánchez, M. J. *Phys. Rev. A* **2018**, *98* (4), 042337.

37. Munyaev, V. O.; Bastrakova, M. V. *Phys. Rev. A* **2021**, *104*, 012613. doi:10.1103/PhysRevA.104.012613.

38. Gramajo, A. L.; Domínguez, D.; Sánchez, M. J. *Phys. Rev. A* **2021**, *104*, 032410. doi:10.1103/PhysRevA.104.032410.

39. Moskalenko, I.; Besedin, I.; Simakov, I.; Ustinov, A. *Applied Physics Letters* **2021**, *119* (19), 194001.

40. Moskalenko, I. N.; Simakov, I. A.; Abramov, N. N.; Grigorev, A. A.; Moskalev, D. O.; Pishchimova, A. A.; Smirnov, N. S.; Zikiy, E. V.; Rodionov, I. A.; Besedin, I. S. *npj Quantum Information* **2022**, *8* (1), 130.

41. Bowdrey, M. D.; Oi, D. K.; Short, A.; Banaszek, K.; Jones, J. *Phys. Lett. A* **2002**, *294* (5), 258–260. doi:https://doi.org/10.1016/S0375-9601(02)00069-5.

42. Albash, T.; Boixo, S.; Lidar, D. A.; Zanardi, P. *New Journal of Physics* **2012**, *14* (12), 123016.

43. Kerskens, C. M.; Pérez, D. L. *Journal of Physics Communications* **2022**, *6* (10), 105001.